

MEASURING AGGLOMERATION OF AGGLOMERATED PARTICLES PICTURES

SHIGEKI MATSUTANI, YOSHIYUKI SHIMOSAKO

ABSTRACT. In this article, we introduce a novel geometrical index δ_{agg} , which is associated with the Euler number and is obtained by an image processing procedure, for a given digital picture of aggregated particles such that δ_{agg} exhibits the degree of the agglomerations of the particles. In the previous work (Matsutani, Shimosako, Wang, Appl.Math.Modeling **37** (2013), 4007-4022), we proposed an algorithm to construct a picture of agglomerated particles as a Monte-Carlo simulation whose agglomeration degree is controlled by $\gamma_{\text{agg}} \in (0, 1)$. By applying the image processing procedure to the pictures of the agglomeration particles constructed following the algorithm, we show that δ_{agg} statistically reproduces the agglomeration parameter γ_{agg} .

agglomeration, digital image processing procedure, Euler number

1. INTRODUCTION

Nano-composite materials have a promising future from industrial viewpoints, since in the materials, geometrical properties in micro-scale plays crucial roles and generates novel and various macro-material properties. By controlling the geometrical properties or shapes, we can design the macro-material properties drastically. Following Kelvin philosophy of science and technology, [K]¹, it is quite important to evaluate such geometrical properties or shapes if one requires to control them.

On the other hand, the smaller the particle is, the larger the effect of the surface energy is. It means that small particles are apt to aggregate or agglomerate in general because the agglomeration and aggregation of the particles decrease the total surface energy and contributes to the stability of the system. When we handle materials consisting of nano-particles, the agglomeration and the aggregation are ones of the most important shapes and sometimes have an effect on the generations of the macro-materials properties. Thus we must pay our attentions on the agglomeration and/or aggregation of particles when we deal with small particles. It is said that the aggregation is due to chemical effects whereas the agglomeration is due to physical effects. Since in a computational model, there is no difference between them, we call both agglomeration in this article, though in

spatial point analysis [IPSS], the aggregation is chosen in general.

In the article [MSW2], in order to find the agglomeration effect in the electric conductivity of the nano-composite material, we study the electric conductivity in an agglomerated continuum percolation model and show that the agglomeration of particles affects the macro-material properties. The purpose of this article is to evaluate the agglomeration in the binary digital images of agglomerated particles, e.g., of electron-microscopes.

For the same purpose, so many evaluation methods and definitions of the agglomeration are proposed to evaluate the agglomeration. In spatial point analysis, the distribution of the nearest distance particles, Clark-Evans index and so on are considered [CE, IPSS]. Further Miles considered the problem in [Mi] and showed the overlapping ratio of the random configurations. These investigations on the agglomeration have been done in the statistical analysis for a point pattern $\mathcal{R} = \{p_i \in \mathbb{R}^2\}$ which are given as statistical configurations of (finite) points. In the analysis, $\mathcal{R}_r := \overline{\bigcup_{p \in \mathcal{R}} U_{r,p}}$ is investigated, which is a configuration of disks whose centers are \mathcal{R} , where $U_{\varepsilon,p} := \{q \in \mathbb{R}^2 \mid |q - p| < \varepsilon\}$. The Euler number, the area and the perimeter of \mathcal{R}_r for several point processes \mathcal{R} 's are computed as morphological indexes or the Minkowski characterization [IPSS]. When \mathcal{R} is given by the point process of the Poisson type, Stoyan, Kendall and Mecke studied their behaviors based on the study of Miles [Mi] and found that

$$(1) \quad e(x) = (1-x)e^{-x}, \quad a(x) = \frac{1}{x}(1-e^{-x}), \quad \ell(x) = e^{-x},$$

where $e(x)$, $a(x)$, and $\ell(x)$ are the normalized versions of the Euler number, the area and the perimeter of \mathcal{R}_r , and x is a normalized radius r [SKM, MS]. Mecke and Stoyan studied

¹ Kelvin wrote his philosophy of science and technology, "In physical science the first essential step in the direction of learning any subject is to find principles of numerical reckoning and practicable methods for measuring some quality connected with it. I often say that when you can measure what you are speaking about, and express it in numbers, you know something about it; but when you cannot measure it, when you cannot express it in numbers, your knowledge is of a meagre and unsatisfactory kind; it may be the beginning of knowledge, but you have scarcely in your thoughts advanced to the state of Science, whatever the matter may be." [K]

the difference among point patterns given by different processes in terms of these behaviors [MS]. Further Tscheschel and Stoyan also studied the statistical reconstruction of random point patterns [TS].

However in the nano-composite materials consisting of nano-particles, the particles themselves sometimes have complicated shapes, such as ellipsoids and rods, as we investigated in [MSW1]. In other words, the configuration is not given by point pattern with radius r in general and thus it is an ill-defined problem, in general, to define the center points of actual agglomerated particles in a given picture, e.g., of an electron-microscopes.

Thus it is natural to consider geometrical properties of the binary picture as a general geometrical object embedded in \mathbb{R}^2 .

Recently MacPherson and Schweinhart proposed a novel method which evaluate the complicatedness of the complicated geometric objects embedded in a plane \mathbb{R}^2 in terms of the persistent homology [MPS]. The persistent homology gives the homological quantities of the filtered persistent modules with real parameter [EH, W]. It could be regarded as a generalization of homotopical approach in traditional algebraic topology [BT], though the deformation does not preserve homotopical properties. For a geometrical object $\mathcal{M} \subset \mathbb{R}^2$, we consider a family of objects with a real parameter $t \in [0, 1]$, i.e., $\{\mathcal{M}_t \mid t \in [0, 1]\}$.

By considering union of the ε -neighborhood of each point in \mathcal{M} , $\mathcal{M}_\varepsilon := \bigcup_{p \in \mathcal{M}} U_{\varepsilon,p}$, induced from the standard Euclidean topology, MacPherson and Schweinhart evaluated the complexity of the geometrical objects. The persistent homology shows the distributions of topological changes generated by counting the Betti number (the homological dimensions) of the filtered persistent modules (vector spaces) induced from $\mathcal{M}_{t'} \subset \mathcal{M}_t$ for $t' < t$.

Following the philosophy of [MPS], to investigate the effect from the standard topology of Euclidean space and to evaluate the complexity, we propose a digital image processing procedure which characterizes the shapes in pictures of the electric microscope in this article. (In Section 3, we give the list of assumed geometrical features of the pictures which we deal with.) For an appropriate geometrical object \mathcal{M} in \mathbb{R}^2 with a characteristic length ℓ , we also handle the family of geometrical objects $\{\mathcal{M}_t = \bigcup_{p \in \mathcal{M}} U_{t,p} \mid t \in [0, \ell]\}$. We define the cumulus of the absolute differential Euler number (CADE) by,

$$(2) \quad \mathcal{E}(\mathcal{M}, \ell) := \int_0^\ell |\chi(\mathcal{M}_t)| dt$$

where $\chi(X)$ is the Euler number of X . $\mathcal{E}(\mathcal{M}, \ell)$ evaluates how many topology changes occur for the deformation $[0, \ell]$.

As we are concerned with the image processing procedure for images of the electron-microscopes, we will customize $\mathcal{E}(\mathcal{M}, \ell)$ as $\hat{\mathcal{E}}(\mathcal{M}, \ell)$ for any binary pictures as an image processing procedure, which is shown in Section 3 more precisely. Further in the nano-materials, there are several scales and one of them is the size of the particles. We fix ℓ and a half of the (average) radius ρ of the particle to evaluate the agglomeration and propose an agglomeration index,

$$(3) \quad \delta_{\text{agg}}(\mathcal{M}) := \frac{\alpha}{\hat{\mathcal{E}}_p(\mathcal{M})} (\hat{\mathcal{E}}_{p(\mathcal{M})} - \hat{\mathcal{E}}(\mathcal{M}, \rho/2)),$$

where $p(\mathcal{M})$ is the volume fraction of \mathcal{M} in the region \mathcal{W} ($\mathcal{M} \subset \mathcal{W} \subset \mathbb{R}^2$), $\hat{\mathcal{E}}_p$ is the average of a ‘‘standard pattern of volume fraction’’ p as mentioned in Section 3, and α is a normalized factor 1.2.

In order to estimate our agglomeration parameter δ_{agg} , we performed Monte-Carlo simulations for the given binary agglomeration configurations of particles whose degree of the agglomeration are parameterized γ_{agg} , since in the article [MSW2], we proposed a statistical model which numerically generates the agglomeration of particles controlled by the parameter γ_{agg} . In Section 2, we review the algorithm following the article [MSW2]. For a given parameter $\gamma_{\text{agg}} \in [0, 1]$, we can statistically construct the infinitely many configuration with the same level of the agglomerations in order to investigate the properties of the agglomerated continuum percolation models. As the continuum percolation model is the same as a germ-grain model in the field of study for the point process [IPSS], there are several other algorithm to construct aggregational germ-grain models, such as Neyman-Scott processes [IPSS], though they are different from ours. These methods are related to agglomeration using artificial clusters, whereas ours are more natural for the actual pictures of electron-microscopes of the agglomerated nano-composite materials as mentioned in [MSW2]. We apply the index δ_{agg} to evaluate the agglomeration of the agglomerated configuration which is generated by the forward method in [MSW2]. Then the relevancy between δ_{agg} and γ_{agg} is shown in Section 4, i.e., in Figure 5 (b) and Table 3. We also mention the relation among our δ_{agg} and the well-established Clark-Evans index in Section 4.

2. AGGLOMERATE CONFIGURATION

In order to explain what is the agglomeration that we are concerned with, we show the agglomeration configurations in computer science, which we handled in [MSW2]. In the article [MSW2], we proposed a construction of the agglomerated continuum percolation models which apparently recovers geometric properties of real nano-particles, though there are several other agglomerated percolation models such as

Neyman-Scott processes [IPSS, SKM, TS]. Since our method has a single parameter γ_{agg} whereas others need several parameters, we believe that ours is more natural than others. As shown in Figure 2, we have the agglomerated configuration of particles depending upon an agglomeration parameter $\gamma_{\text{agg}} \in [0, 1]$. In this section, we show the geometrical setting of agglomerated continuum percolation model in [MSW2], which is modeled by the agglomerated clusters in nature.

We set particles parameterized by their center positions (x, y) into a box-region $\mathcal{W} := [0, L] \times [0, L]$ at random and get a configuration \mathcal{M}_n as a model of continuum percolation. The particle corresponds to a disk with the same radius ρ , $B_{x_i, y_i} := \{(x, y) \in \mathcal{W} \mid |(x, y) - (x_i, y_i)| \leq \rho\}$. The configuration \mathcal{M}_n is given by $\mathcal{M}_n := \bigcup_{i=1}^n B_{x_i, y_i}$.

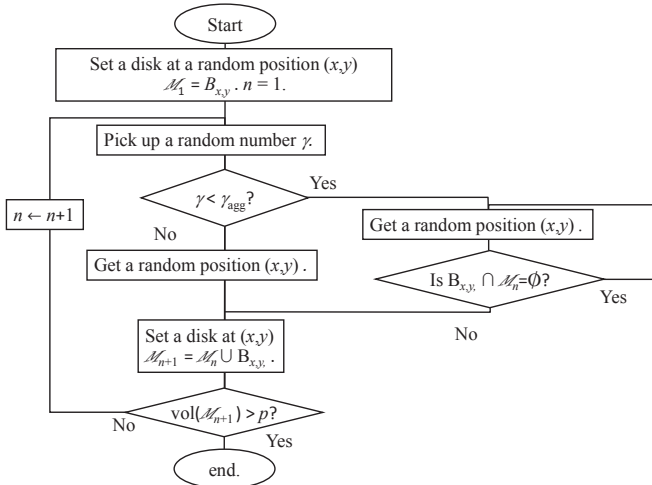


FIGURE 1. The flowchart of the agglomeration configuration algorithm.

The flowchart in Figure 1 illustrates the algorithm. As an initial state, the configuration \mathcal{M}_0 has no particle. As the first step, for a uniform random position $(x, y) \in \mathcal{W}$, we set a particle $B_{x,y}$ whose center is (x, y) and the radius is ρ , i.e., $\mathcal{M}_1 := B_{x,y}$.

For $(n + 1)$ -step, we take a position (x, y) at uniform random in \mathcal{W} , and another random parameter γ at uniform random in $[0, 1]$. If γ is greater than γ_{agg} , we set $\mathcal{M}_n := \mathcal{M}_n \cup B_{x,y}$. We now allow the particles to overlap each other.

For the case $\gamma \leq \gamma_{\text{agg}}$, we first check whether the disk $B_{x,y}$ is connected with the previous configuration \mathcal{M}_n or not. For the case $\mathcal{M}_n \cap B_{x,y} \neq \emptyset$, we employ the position and set $\mathcal{M}_{n+1} := \mathcal{M}_n \cup B_{x,y}$. Otherwise or $\mathcal{M}_n \cap B_{x,y} = \emptyset$, we abandon the position and go on to take another uniformly random position (x, y) in \mathcal{W} until we find the position which supplies a connected particle $B_{x,y}$ with \mathcal{M}_n .

In other words, for the case $\gamma \leq \gamma_{\text{agg}}$, the added particle must be connected with the previous configuration \mathcal{M}_n . Thus, γ_{agg} stands for the agglomeration of the particle system.

By monitoring the total volume fraction which is a function of \mathcal{M}_n and is denoted by $p(\mathcal{M}_n)$, we go on to put the particles as long as $p(\mathcal{M}_n) \leq p$ for a given volume fraction p . We find the step $n(p)$ such that $p(\mathcal{M}_{n(p)-1}) \leq p$ and $p(\mathcal{M}_{n(p)}) > p$. Since we assume that the difference between $p(\mathcal{M}_{n(p)-1})$ and $p(\mathcal{M}_{n(p)})$ is sufficiently small, we regard $p(\mathcal{M}_{n(p)})$ as the volume fraction p itself hereafter under this accuracy.

Since in the Monte-Carlo method, we use the pseudo-randomness to simulate the random configuration $\mathcal{M}_{n(p)}$ for given p and γ_{agg} , the configuration $\mathcal{M}_{n(p)}$ depends upon the seed i_S of the pseudo-randomness which we choose. We let it be denoted by $\mathcal{M}_{\gamma_{\text{agg}}, p, i_S}$ or its statistical quantity by $\mathcal{M}_{\gamma_{\text{agg}}, p}$.

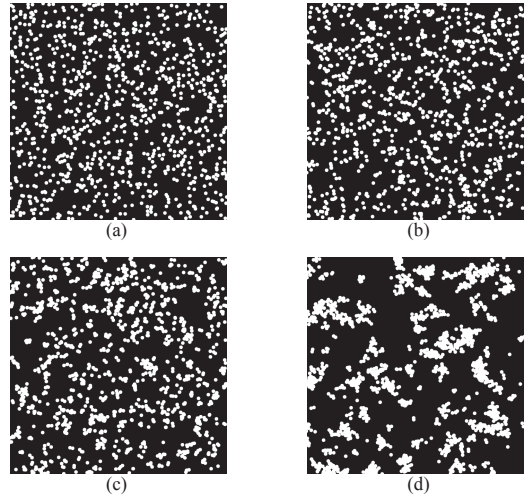


FIGURE 2. The agglomeration configuration: Two-dimensional random particle system of $p = 0.2$ with the agglomeration parameter $\gamma_{\text{agg}} = 0.0, 0.3, 0.6$ and 0.9 for (a), (b), (c), and (d) respectively.

For sufficiently large L and L' ($\rho \ll L' < L$) and for a window $\mathcal{W}'_{(x,y)} := [x, x + L'] \times [y, y + L'] \subset \mathcal{W}$, the volume fraction $p'(x, y)$ in $\mathcal{W}'_{(x,y)}$ is proportional to the number of particles $N'(x, y)$ in $\mathcal{W}'_{(x,y)}$, i.e., there is a constant number λ such that $p'(x, y) = \lambda N'(x, y)$. Further $\mathcal{M}_{\gamma_{\text{agg}}, p, i_S}$ is isotropic and independently scattered and thus $\mathcal{M}_{\gamma_{\text{agg}}, p, i_S}$ is a kind of Poisson process [IPSS, p.66].

Further though our algorithm is not Markov process because each step depends on the previous configuration, we should note that it preserves a hierarchical structure for

fixed i_S and $p > p'$,

$$\mathcal{M}_{\gamma_{\text{agg}}, p', i_S} \subset \mathcal{M}_{\gamma_{\text{agg}}, p, i_S}.$$

As we will show the assumed geometric properties of pictures in Section 3, the pictures which we will deal with are illustrated in Figure 2. Figure 2 displays the configurations following our algorithm. Our more concrete aim of this article is to recover the γ_{agg} for a given configuration $\mathcal{M}_{\gamma_{\text{agg}}, p}$ in a statistical meaning. More precisely, our study is to find a statistical monotone function of γ_{agg} and to show that one of them is δ_{agg} in (3).

3. EVALUATION OF AGGLOMERATION FOR A CONFIGURATION $\mathcal{M}_{p, \gamma_{\text{agg}}} \subset \mathcal{W}$

As we are concerned with the evaluation method as a digital image processing procedure [P], in this section, we illustrate our algorithm for a picture which only has binary values. It is natural that we assume the configuration \mathcal{M} (implicitly $\mathcal{M}_{p, \gamma_{\text{agg}}, i_S}$ and a picture of nano-composite material in an electron-microscope) has the following structures:

- (1) L is sufficiently larger than ρ so that the particles of \mathcal{M} are a representative of sufficiently randomized configurations; We could assume the Euclidean invariance (translation, rotation and inversion) statistically; after averaging them, the physical and geometrical quantities are invariant for any Euclidean action $\text{SE}(2)$ up to the statistical deviation. If the deviation is not small, we could consider the series of $\{\mathcal{M}_{p, \gamma_{\text{agg}}, i_S} \mid i_S\}$. (It means that for the case of the pictures of the electron-microscopes, we could assume that the researchers prepare the series of pictures of a material or materials which are produced in the same conditions.)
- (2) It is assumed that the volume fraction is less than the percolation threshold of two dimensional continuum percolation models. (For the case of nano-composite material which is based upon the percolation theory, the volume fraction around the percolation threshold $0.2 \sim 0.3$ is concerned, which is far less than the percolation threshold of two dimensional case $0.5 \sim 0.7$.)
- (3) There are three sizes of the system or the picture $\mathcal{M}_{p, \gamma_{\text{agg}}}$ (and the digital image of nano-composite material of an electron-microscope);
 - (a) the (average) size of particles, which is given as ρ ,
 - (b) the analyzed size of the system, which is, now, given by L as mentioned above, and
 - (c) the pixel size a , which is also controlled so that we can discriminate the particles concerned level.

Under these assumptions, we consider geometry of \mathcal{M} . It is known that the ε -neighborhood, $\mathcal{M}_\varepsilon = \bigcup_{p \in \mathcal{M}} U_{\varepsilon, p} \cap \mathcal{W}$,

can be realized by the so-called level set method in computer science [S]. Let $d : \mathcal{W} \rightarrow \mathbb{R}$ be the signed distance from the boundary $\partial\mathcal{M}$ so that the outer side is assigned to the positive distance and the inner side is to the negative one, and then the geometrical object in the level set method can be regarded as $\mathcal{L}_t = d^{-1}(t)$. \mathcal{M}_t of ($t > 0$) is equal to $d^{-1}([0, t]) \cup \mathcal{M}$ and $\mathcal{L}_t = \partial\mathcal{M}_t$. For $t < 0$ case, $\mathcal{L}_t = \partial(\bigcup_{p \in \partial\mathcal{M}} U_{t, p}) \setminus \mathcal{L}_{-t}$. Hence by means of the level set method, we can compute the more precise geometrical properties beyond the pixel size resolution even on the image defined over a subset of \mathbb{Z}^2 .

However in the digital image processing procedure, we investigate the geometrical object up to the pixel size resolution in general. Hence in this article, we use the thickening scheme in the image processing procedure [P] instead of the level set function. Though the ordinary thickening scheme has anisotropic behavior, it does not have a serious effect on the result because the configuration itself is isotopic or rotational invariant. We use the modified thickening scheme, which improves the anisotropic behavior shown in Section 4. Let $\mathcal{M}^{(i)}$ be the i -th thickening of \mathcal{M} in \mathcal{W} . We modify the CADE (2) as an image processing procedure by

$$\hat{\mathcal{E}}(\mathcal{M}, na) := a \sum_{i=1}^{\rho/2a} |\chi(\mathcal{M}^{(i)}) - \chi(\mathcal{M}^{(i-1)})|.$$

For the case $na < \rho$, the anisotropy due to the thickening is not large and thus we regard $\mathcal{M}^{(i)}$ as \mathcal{M}_{ai} .

In the persistent homology, the Betti number is handled in general. In the complicated system, we believe that it is quite important how many topology changes occur for the i -step and thus, we consider the Euler number. Further more precisely there is no guaranteed that $\chi(\mathcal{M}_t)$ is equal to $\chi(\mathcal{M}^{(i-1)})$ for $t \in [a(i-1/2), a(i+1/2))$. However as mentioned above, in digital analysis, we should basically neglect finer geometrical difference than the pixel size resolution and we follow the principle.

Further the agglomeration can be discriminated whether the particles are connected or not. From (1), if L/ρ is sufficiently large, even for $\gamma_{\text{agg}} = 0$ and small p , $\hat{\mathcal{E}}(\mathcal{M}_{0, p}, na)$ does not vanishes $n > 0$, in general, due to the randomness of the configurations. Further the behavior $\hat{\mathcal{E}}(\mathcal{M}, na)$ of $n \in [0, \rho/2a)$ is quite important since the agglomeration suppresses the topology change in the interval as illustrated in Figure 4. Due to the randomness of the configurations, it is not so important whether the Euler numbers increase or decrease, but it is much important that the topological change for the deformation is quite important.

We define the agglomeration parameter δ_{agg} in (3) more precisely

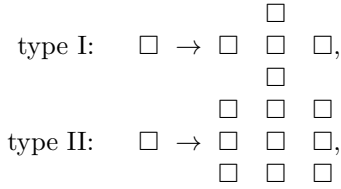
$$(4) \quad \delta_{\text{agg}}(\mathcal{M}) = \frac{\alpha}{\hat{\mathcal{E}}_p(\mathcal{M})} (\hat{\mathcal{E}}_p(\mathcal{M}) - \hat{\mathcal{E}}(\mathcal{M}, \rho/2)),$$

where $p(\mathcal{M})$ is the volume fraction of \mathcal{M} , $\hat{\mathcal{E}}_p$ is the average of the standard patterns of volume fraction p , and α is a normalized factor 1.2, which is chosen as a result of the comparison with γ_{agg} (see Table 3). The standard pattern means the pattern of $\gamma_{\text{agg}} = 0$ with the same radius in the same window \mathcal{W} . Then $\delta_{\text{agg}}(\mathcal{M}_{\gamma_{\text{agg}},p})$ characterizes how many topological changes occurs for the deformations for each particle in $\mathcal{M}_{\gamma_{\text{agg}},p}$ by normalized by $\hat{\mathcal{E}}_p$. It shows the Figure 3.

4. NUMERICAL COMPUTATION AND RESULTS

Let us show the relevance between δ_p and γ_p by the Monte-Carlo simulations following the algorithm mentioned in Section 2. Using the algorithm in Section 2, we have ten pictures of agglomerated particles for each $\gamma_{\text{agg}} = 0, 0.3, 0.6$ and 0.9 , and for each $p = 0.1, 0.2, 0.3$ and 0.4 by letting $L = 2400$ and $\rho = 20$ as in Figure 2.

On the thickening to compute CADE, we use two types thickening process;



which generate an octagon asymptotically and approximates the area of the disks; in other words, on the thickening pro-

TABLE 1. The pattern of thickening

steps	type	radius	area	n.of pixels
1	II	0.5	0.785	1
2	I	1.5	7.065	9
3	I	2.5	19.625	21
4	I	3.5	38.465	37
5	II	4.5	63.585	69
6	I	5.5	94.985	97
7	I	6.5	132.665	129
8	II	7.5	176.625	185
9	I	8.5	226.865	229
10	I	9.5	283.385	277

cess, we use the deformation in digital process procedure for each point which is given in Table 1. Further for each point,

we consider the thickening:

```

      0 0 0 0 0 0 0 0
    0 9 9 9 9 9 9 9 0
      0 9 8 8 8 8 8 8 9 0
    0 9 8 8 7 6 6 6 6 7 8 8 9 0
  0 9 8 8 7 6 5 5 5 5 5 6 7 8 8 9 0
0 9 8 8 7 6 5 5 4 4 4 5 5 6 7 8 8 9 0
0 9 8 7 6 5 4 3 3 3 3 4 5 5 6 7 8 9 0
0 9 8 7 6 5 4 3 2 2 2 3 4 5 6 7 8 9 0
0 9 8 7 6 5 4 3 2 1 2 3 4 5 6 7 8 9 0
0 9 8 7 6 5 4 3 2 2 2 3 4 5 6 7 8 9 0
0 9 8 7 6 5 4 3 3 3 3 4 5 5 6 7 8 9 0
0 9 8 8 7 6 5 5 4 4 4 5 5 6 7 8 8 9 0
  0 9 8 8 7 6 5 5 5 5 5 6 7 8 8 9 0
    0 9 8 8 7 6 6 6 6 6 7 8 8 9 0
      0 9 8 8 7 7 7 7 7 8 8 9 0
        0 9 8 8 8 8 8 8 8 9 0
          0 9 9 9 9 9 9 9 0
            0 0 0 0 0 0 0 0

```

We computed the ten pictures for each $p = 0.1, 0.2, 0.3, 0.4$ and $\gamma_{\text{agg}} = 0.0, 0.3, 0.6, 0.9$ with ten random seeds. Figure 3 shows the CADE and the thickening step ℓ for each p .

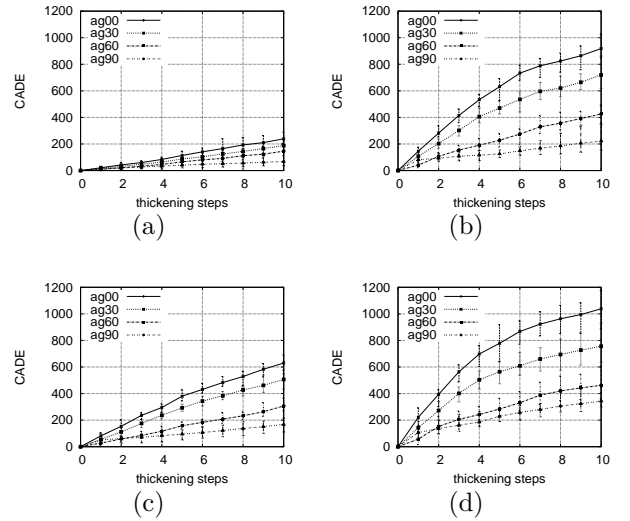


FIGURE 3. The CADE vs thickening steps ℓ for different γ_{agg} ; The graphs of the volume fraction $p = 0.1, 0.2, 0.3$ and 0.4 are illustrated in (a), (b), (c), and (d) respectively.

On the other hand, though it is difficult to identify the center points of the particles for given pictures, especially of the agglomerated case as shown in Figure 2 (b) and (c), we know the data of the center points of the particles. Thus we can use the techniques of the statistical analysis for the spatial point patterns. Figure 4 displays the global distribution of the Euler numbers of different radius of a seed by using the software provided in [IPSS, p.204]². Since our radius is 20 and our agglomeration algorithm is characterized by the radius, the behavior of the distribution differs depending on

² <http://www.maths.jyu.fi/~penttine/ppstatistics>.

the regions $\rho > 20$ and $\rho \leq 20$. Figure 3 correspond to (20, 30] region and thus it implies that our improved thickening algorithm works well. Since the agglomeration in our algorithm means that the number of agglomerated particles is larger than the uniform randomness $\gamma_{\text{agg}} = 0$. The variation of the Euler number is related to the deformation in which disjoint clusters connect due to the thickening. Agglomeration means that the number of the disjoint clusters is less than that of uniform randomness. The variation of the Euler number for the increasing of the radius $\rho > 20$ is suppressed for large γ_{agg} . Hence the dependence in Figure 3 is very natural.

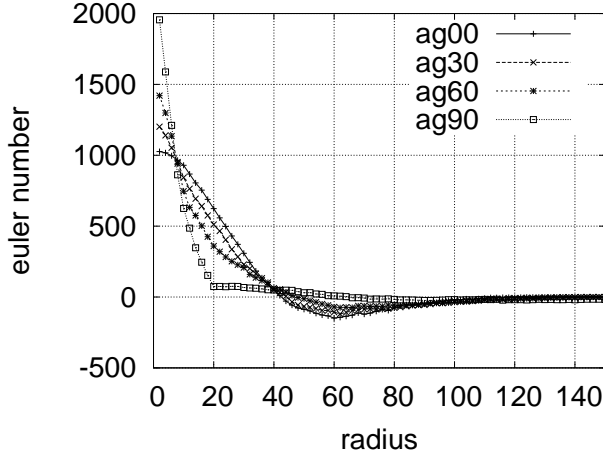


FIGURE 4. The Euler number vs the radius ρ as the point pattern of $\mathcal{M}_{\gamma_{\text{agg}}, p, i_S}$ of $p = 0.2$ and a certain i_S .

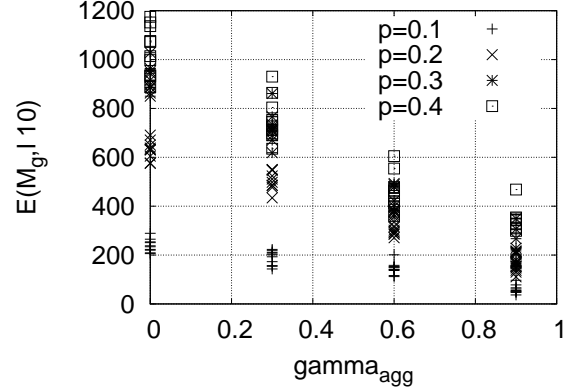
In order to find these behaviors more precisely, we consider the dependence of CADE $\hat{\mathcal{E}}(\mathcal{M}_{\gamma_{\text{agg}}, p, i_S}, \rho/2)$ on the agglomeration parameter γ_{agg} .

Table 2 and Figure 5 (a) show the dependence of CADE $\hat{\mathcal{E}}(\mathcal{M}_{\gamma_{\text{agg}}, p}, \rho/2)$ on the agglomeration parameter γ_{agg} for each p . They exhibit the negative correlations. The agglomeration means that the number of agglomerated particles is larger than the uniform randomness $\gamma_{\text{agg}} = 0$ as mentioned above. Since the agglomeration prevents the topological changes for the thickening, we have the negative correlation in Figure 5 (a).

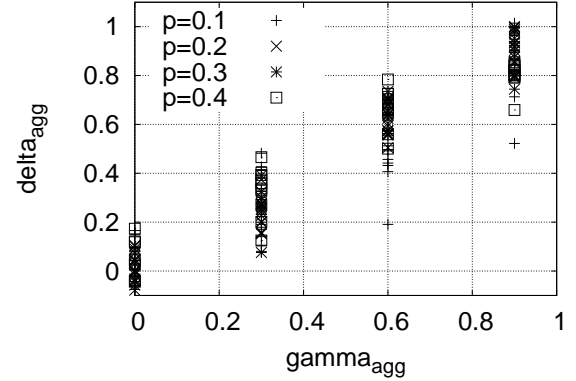
We, now, define the $\hat{\mathcal{E}}_p$ by the average of CADE $\hat{\mathcal{E}}(\mathcal{M}_{i_S}, \rho/2)$ of the uniform random configuration, i.e., $\gamma_{\text{agg}} = 0$ case,

$$\hat{\mathcal{E}}_p := \frac{1}{10} \sum_{i_S=1}^{10} \hat{\mathcal{E}}(\mathcal{M}_{0, p, i_S}, \rho/2).$$

Further in order that δ_{agg} corresponds to γ_{agg} , we chose $\alpha = 1.2$. Figure 5 (b) and Table 3 show the relation between δ_{agg} and γ_{agg} :



(a)



(b)

FIGURE 5. The CADE of $\rho/2$ and the agglomeration index δ_{agg} vs γ_{agg} .

TABLE 2. CADE vs γ_{agg} :

p	0.1			0.2		
	Ave	Max	Min	Ave	Max	Min
0	238.9	289	206	630.1	691	575
0.3	187.8	223	143	506.1	550	434
0.6	145.7	201	112	306.5	365	271
0.9	67.8	135	37	167.6	215	111
p	0.3			0.4		
	Ave	Max	Min	Ave	Max	Min
0	918.5	1028	850	1038.1	1175	888
0.3	720	861	619	756.1	930	635
0.6	425.7	493	356	461.8	605	360
0.9	222	349	153	343.4	468	299

Table 3 show that γ_{agg} recovers δ_{agg} for the given pictures up to the statistical fluctuation.

TABLE 3. δ_{agg} vs γ_{agg} :

p	0.1			0.2		
γ_{agg}	Ave	Min	Max	Ave	Min	Max
0	0.000	-0.270	0.177	0.000	-0.124	0.112
0.3	0.275	0.086	0.516	0.253	0.163	0.400
0.6	0.502	0.204	0.683	0.660	0.541	0.733
0.9	0.921	0.559	1.087	0.944	0.847	1.059
p	0.3			0.4		
γ_{agg}	Ave	Min	Max	Ave	Min	Max
0	0.000	-0.154	0.095	0.000	-0.170	0.186
0.3	0.277	0.080	0.419	0.349	0.134	0.499
0.6	0.689	0.595	0.787	0.714	0.536	0.840
0.9	0.975	0.797	1.071	0.860	0.706	0.915

In the statistical analysis of the spatial point patterns, the Clark-Evans index is a well-established index which represents the agglomeration degree of a given point pattern, though in general, it is very difficult to identify the center points of the particles for a given picture, such as Figure 2 (b) and (c). Since we know the data of the center points of the particles of every $\mathcal{M}_{\gamma_{\text{agg}}, p, i_S}$, we illustrated the Clark-Evans index as follows:

TABLE 4. Clark Evans index vs γ_{agg} :

p	0.1			0.2		
γ_{agg}	Ave	Max	Min	Ave	Max	Min
0.0	1.019	1.040	0.977	1.027	1.062	1.007
0.3	0.713	0.763	0.676	0.784	0.818	0.767
0.6	0.465	0.501	0.427	0.622	0.637	0.607
0.9	0.341	0.358	0.331	0.526	0.538	0.511
p	0.3			0.4		
γ_{agg}	Ave	Max	Min	Ave	Max	Min
0.0	1.016	1.034	1.002	1.019	1.032	1.007
0.3	0.858	0.875	0.847	0.908	0.920	0.893
0.6	0.738	0.751	0.719	0.819	0.831	0.808
0.9	0.638	0.648	0.630	0.726	0.746	0.714

The Clark-Evans index represents our agglomeration parameter γ_{agg} well. The correlation between the Clark-Evans index and δ_{agg} is displayed in Figure 6. They show good negative-correlations for each volume fraction p .

However our method has advantage because we don't need to find the center points. though the determination of the center points of the particles is basically an ill-posed problem for a given picture such as Figure 2 (b) and (c). In other words, our purpose which we recover γ_{agg} for a given picture by means of the digital image processing procedure is accomplished by following the philosophies of the study of persistent homology [MPS].

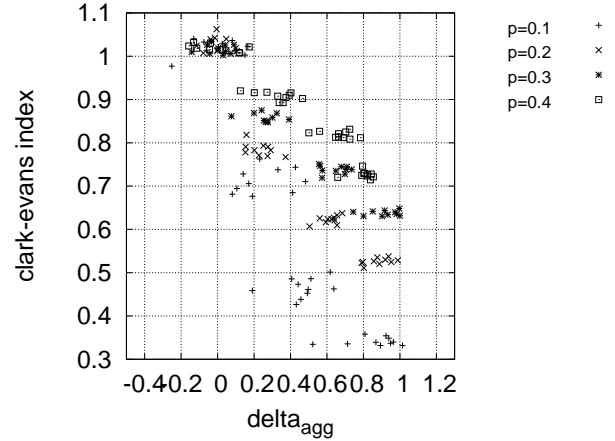


FIGURE 6. The Clark-Evans index and δ_{agg} .

REFERENCES

- [BT] R. Bott and L. W. Tu, *Differential Forms in Algebraic Topology*, (GTM 82) Springer, Berlin, 1982.
- [CE] P. J. Clark and C. Evans, *Distance to Nearest Neighbor as a Measure of Spatial Relationships in Populations*, *Ecology*, **35** (1954) 445-453.
- Differential Forms in Algebraic Topology, (GTM 82) Springer, Berlin, 1982.
- [EH] H. Edelsbrunner and J. Harer, *Persistent homology: A survey*, in *Surveys on Discrete and Computational Geometry. Twenty Years Later*, 257282 (J. E. Goodman, J. Pach, and R. Pollack, eds.), Contemporary Mathematics 453, Amer. Math. Soc., Providence, Rhode Island, 2008.
- [HSWNS] L. Hui, R. C. Smith, X. Wang, J. K. Nelson and L. S. Schadler, *Quantification of Particulate Mixing in Nanocomposites*, 2008 Annual Report Conference on Electrical Insulation Dielectric Phenomena, IEYASU, (2008) 317-320.
- [K] B. Kelvin, *Electrical Units of Measurement*, Popular Lectures and Addresses Volume I, London: Macmillan and Co., 1889, pp. 73-74.
- [IPSS] J. Illian, A. Penttinen, H. Stoyan, D. Stoyan, *Statistical Analysis and Modelling of Spatial Point Patterns (Statistics in Practice)*, Wiley, New York, 2008.
- [MPS] R. MacPherson and B. Schweinhart, *Measuring shape with topology*, *J. Math. Phys.*, **53** (2012) 073516(13 pages).
- [MS] K. R. Mecke and D. Stoyan, *Morphological Characterization of Point Patterns*, *Biometrical J.*, **47** (2005) 473-488.
- [MSW1] S. Matsutani, Y. Shimosako, and Y. Wang, *Numerical Computations of Conductivity in Continuum Percolation for Overlapping Spheroids*, *Int. J. Mod. Phys. C*, **21** (2010) 709-729.
- [MSW2] S. Matsutani, Y. Shimosako, and Y. Wang, *Numerical Computations of Conductivities over Agglomerated Continuum Percolation Models*, *Appl. Math. Modeling*, **37** (2013) 4007-4022.
- [Mi] R. E. Miles, *Estimating aggregate and overall characteristics from thick sections by transmission microscopy*, *J. of Microscopy*, **107** (1976) 227-729.
- [P] W. K. Pratt, *Digital Image Processing*, 2nd ed., Wiley, New York, 1991.

- [S] J. A. Sethian, *Level Set Methods and Fast Marching Methods: Evolving Interfaces in Computational Geometry, Fluid Mechanics, Computer Vision, and Materials Science*, Cambridge Univ. Press Cambridge, 1999.
- [SKM] D. Stoyan, W. S. Kendall and J. Mecke, *Stochastic Geometry and its Applications*, 2nd ed., Wiley, New York, 1995.
- [TS] A. Tscheschel and D. Stoyan, *Statistical reconstruction of random point patterns*, *Comp. Stat. Data Anal.*, **51** (2006) 859-871.
- [W] S. Weinberger, *What is Persistent Homology?*, *Notices of the AMS*, **58** (2011) 36-39.

Shigeki Matsutani, Yoshiyuki Shimosako
Simulation & Analysis R&D Center,
Canon Inc., 3-30-2, Shimomaruko Ohta-ku,
Tokyo, Japan